Real-time experimental demonstration of a computationally efficient hybrid OFDM DFMA PON

Giddings, Roger; Tyagi, Tushar; Tang, Jianming

Optical Fiber Technology

DOI:
10.1016/j.yofte.2022.103106

Published: 01/12/2022

Publisher's PDF, also known as Version of record

Optical Fiber Technology 74 (2022) 103106

Contents lists available at ScienceDirect

Optical Fiber Technology

journal homepage: www.elsevier.com/locate/yofte

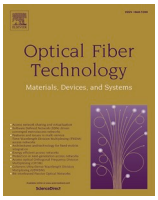

Real-time experimental demonstration of a computationally efficient hybrid OFDM DFMA PON

Tushar Tyagi, Roger Giddings *, J.M. Tang

DSP Centre, School of Computer Science and Electronics Engineering, Bangor University, LL57 1UT, UK

ARTICLE INFO

Keywords:
Orthogonal frequency division multiplexing (OFDM)
digital filter multiple access (DFMA)
passive optical networks (PON)
Hybrid OFDM DFMA PON

ABSTRACT

This paper presents the first real-time experimental demonstration of a hybrid OFDM DFMA PON. The presented PON is validated for two channels (*I* or *Q*) occupying two subwavelength bands. The hybrid OFDM DFMA PON eliminates the need for a dedicated matching filter at the receiver for each individual channel, by employing a single FFT operation to recover all channels, thereby achieving lower computational complexity. The hybrid OFDM DFMA PON used in conjunction with a joint sideband processing technique, when compared to a DFMA PON under the exact same operating conditions, is shown to offer increased performance, including a lower received optical power of up to 1.2 dB for the adopted FEC limit at a given bit rate. The experimentally demonstrated PON is also proven to be significantly more tolerant to the symbol timing offset effect at the OLT receiver. Furthermore, compared to the DFMA PON's OLT receiver, the implemented FFT-based receiver is shown to operate at a drastically reduced logic clock rate and with significantly lower DSP complexity. The hybrid OFDM DFMA PON is thus shown to have numerous advantages over the DFMA PON.

1. Introduction

Recently emerging network services associated with internet of things (IoT), on-demand video streaming, cloud computing and Industry 4.0, all involve billions of devices interacting across the internet to connect machines, users, and data-center clouds to drive consumer and business interactions, which all exacerbate the eruption of demands on the future networks [1]. These new services lead to highly dynamic traffic patterns in the network; however, the conventional network architectures have been designed for accommodating static traffic services with dedicated and fixed bit rates for end-users. The need for low-cost future networks is thus driving the network providers to re-examine their network architectures to support the dynamic, reconfigurable, and flexible requirements of the aforementioned emerging services. To meet the rigorous demands of 5G and beyond mobile networks and the 5th generation of the fixed networks (F5G), cloud access networks (CANs) have been proposed [2], which are designed to be capable of seamlessly converging mobile and fixed networks whilst achieving the required dynamic network operation. A vital element of realising a CAN is the use of highly flexible, reconfigurable and dynamic PON architectures.

To achieve the desired low-cost and sustainable future network solutions, software-defined networking (SDN) with its capabilities extended to the physical layer is highly appropriate, as it can offer efficient control and management of the new network features such as dynamic bandwidth allocation (DBA), adaptive modulation, optimization of network resource utilization, and dynamic on-demand connections/services. In this regard, an SDN compatible, optical orthogonal frequency division multiplexing multiple access (OOFDMA) PON utilizing real-time OOFDM transceivers has been proposed and demonstrated in [3], as it can offer a number of advantages such as high spectral efficiency, adaptive signal modulation according to channel characteristics, DBA with fine bandwidth granularity, trivial equalization through simple complex multiplication per subcarrier, as well as excellent tolerance to channel dispersion (CD) [3,4]. In terms of the implementation of the OFDMA PONs, digital signal processing (DSP) can be utilized to realize highly cost-effective and flexible OFDM transceivers. However, OFDMA PON transceivers for ONUs, suffer from the limitation of high DSP complexity as an IFFT and an FFT are needed to generate and receive all employed OFDM subcarriers, even if one ONU will only use a small subset of the available subcarriers. To overcome these limitations, a digital filter multiple access PON (DFMA PON) architecture was proposed and experimentally verified [5–7]. The DFMA PON implements digital shaping filters (SF) at the transmitter with their

* Corresponding author.
E-mail address: r.p.giddings@bangor.ac.uk (R. Giddings).

https://doi.org/10.1016/j.yofte.2022.103106
Received 6 July 2022; Received in revised form 1 September 2022; Accepted 10 October 2022
Available online 1 November 2022

corresponding digital matching filters (MF) at the receiver so that the different channels can be dynamically configured to share the same transmission medium. The channel manipulation in the digital domain removes the need for expensive RF/optical components. The salient features of the DFMA technique are: (i) Improved dynamic network reconfigurability, ease of network virtualization and channel bandwidth elasticity with SDN control functionalities extended to physical layer, (ii) Inherent backwards compatibility with all existing PONs, (iii) Transparency to signal modulation format, (iv) Enhanced security as full knowledge of filter parameters is required for channel demultiplexing, (v) Good scalability due to the modular nature of the DSP solution in the optical line terminal (OLT), and (vi) The low costs associated with large-scale, mass-produced digital integrated circuits can keep PON capital expenditure (CAPEX) levels commercially viable. Despite the aforementioned features of the DFMA technique, the DFMA PON can suffer from cross-channel interference (CCI) due to imperfect channel orthogonality. The CCI increases as the channel orthogonality degrades; thus, it leads to degraded DFMA PON performance due to unwanted leakage of a channel to its corresponding orthogonal channel. To address this, a cross-channel interference technique has also been proposed and verified in [8] with an online experimental demonstration to further improve the performance of the DFMA PON. This, however, leads to a further burden on the DSP complexity of the DFMA technique. Moreover, as the number of channels increases the required MF and corresponding FFTs at the receiver increase proportionately leaving the DSP complexity a fundamental challenge for high channel counts. Furthermore, the DFMA PON performance is sensitive to non-ideal physical channel responses with significant roll-offs and/or non-ideal digital filter frequency responses. To overcome the aforementioned challenges, the hybrid OFDM DFMA PON has been proposed in [9] wherein a single FFT operation replaces the multiple MFs as well as the individual FFT operations required in the OLT receiver, thereby significantly reducing the DSP complexity. The hybrid OFDM DFMA PON has been analyzed numerically [9] and experimentally verified with off-line signal processing [10] and is shown to offer the following advantages:

- Great relaxation in SF complexity requirement. The insensitivity of the proposed technique to SF-induced signal distortions and channel non-linearities can be exploited to use low complexity SFs in the ONUs thereby reducing the DSP complexity.
- Drastic reduction in the DSP complexity of the OLT receiver by removing the required MFs and multiple FFTs and replacing with a single FFT operation.
- The maximum clock rate required at the OLT is significantly less, which lowers the power requirement from the system on chip (SoC) point of view.
- Enhanced performance compared to the DFMA PON proposed in [8].

However, the real-time practical implementation of the previously proposed hybrid OFDM DFMA PON must be demonstrated to fully validate its technical feasibility. To this end, this paper presents the first experimental demonstration of a real-time hybrid OFDM DFMA PON and thus proves its technical feasibility. A comprehensive analysis of the point-to-point (PTP) case is first presented, followed by the more challenging multipoint-to-point (MPTP) upstream PON transmission case, from ONU to OLT. A comprehensive comparison with a real-time DFMA PON under the same operating conditions is also presented, in terms of bit error rate (BER) performance for the same signal bit rate and sensitivity to the symbol timing offset (STO) at the OLT's receiver. Finally, complexity analysis of the two aforementioned PON's OLT receiver DSPs is presented to study how the complexity scales with the channel count, it is shown that for channel counts of $\sim$ 256 the hybrid OFDM DFMA PON has a lower complexity by a factor of $\sim$ 5 times.

2. Real-time hybrid OFDM DFMA PON transceiver architecture

The implemented 4 channel hybrid OFDM DFMA PON system consists of two channels *I* (Cosine) and *Q* (Sine) per subwavelength (SW) band, with a total 1 GHz bandwidth divided into two SW bands: baseband (0–0.5 GHz) and passband (0.5–1 GHz). The pictorial representation of the divided frequency spectrum is shown in Fig. 1. As seen from Fig. 1, the 4 channels obtained are: cosine baseband (BB-I), cosine passband (PB-I), sine baseband (BB-Q), and sine passband (PB-Q). The DSP architecture of the proposed hybrid OFDM DFMA PON is also shown in Fig. 2.

2.1. Transmitter architecture

The ONU transmitter, as shown in Fig. 2, is implemented in an Intel Stratix IV FPGA and can be dynamically reconfigured to generate either baseband (OFDM source 1) or passband (OFDM source 2) for any of the channels *I* and *Q*. The aforementioned two independent OFDM signal sources can be adaptively modulated to provide 16-QAM, 32-QAM, 64-QAM and 128-QAM signals. The OFDM signal is made up of 40 $\times$ 8 bit parallel samples with a clock rate of 12.5 MHz. To reduce the logic resource utilization, the 40 parallel samples are converted to 4 parallel samples operating at a clock rate of 125 MHz. Up-sampling by a factor of 4 is performed and the resulting multi-image signal, consisting of 16 parallel samples, is passed through 16 parallel shaping filters, to achieve the required signal throughput. The Hilbert pair approach described in [6] is used to design the filters wherein the reconfigurable filter coefficients are assigned 8 bit values. The shaping filters perform the necessary frequency and bandwidth allocation to the incoming OFDM signal, i.e. selecting the desired spectral image. The resulting filter outputs from both channels are then added digitally and to meet the DAC interface requirements, they are subsequently converted to 40 parallel samples at a clock rate of 50 MHz. Thus, the summed signals are transmitted through the DAC interface operating at 2 GS/s. The DAC output directly drives an optical intensity modulator (IM). Further details of the transmitter architecture can be found in [8].

2.2. Receiver architecture

The OLT receiver, as shown in Fig. 2, is implemented in an Intel Stratix V FPGA and can be dynamically reconfigured to detect any one of the four supported channels. In practice, the receiver architecture must of course detect multiple channels simultaneously. In the OLT's direct-detection (DD) receiver, a PIN converts the optical signal back to an electrical signal. The amplified and filtered electrical signal from the PIN is received and digitized at 2 GS/s by an ADC, which produces 40 parallel samples at a clock rate of 50 MHz for processing by the FPGA. Unlike the DFMA OLT receiver, the hybrid OFDM DFMA OLT receiver eliminates the multiple MFs and associated FFTs by replacing them all with a single FFT operation. The size of the FFT '*L*' required is dependent on the up-sampling factor *M* and the IFFT size *N* at the transmitter as $L = M \times N = 4 \times 32 = 128$ [9]. The 40 received parallel samples are

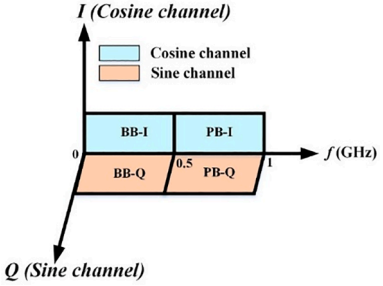

Fig. 1. Bandwidth allocation for the different channels.

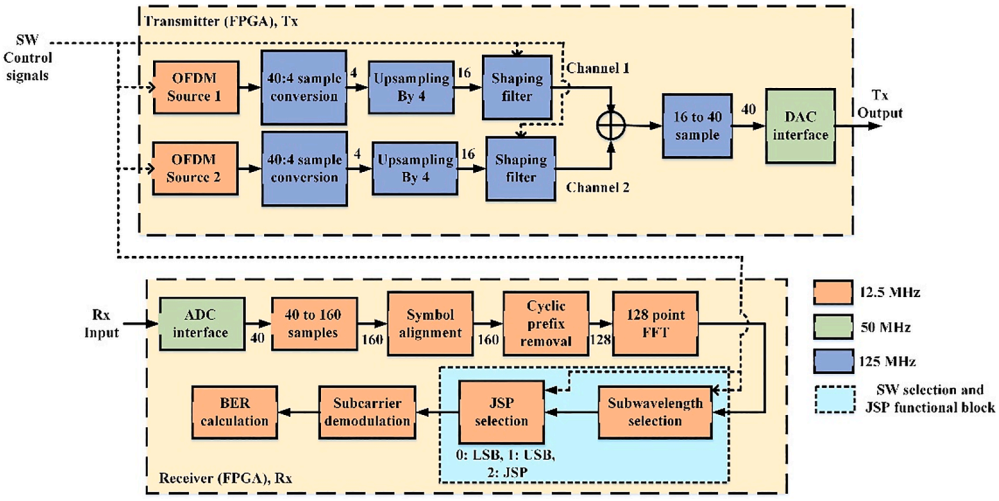

Fig. 2. DSP architecture of hybrid OFDM DFMA PON.

converted to 160 parallel samples, clocked at 12.5 MHz. The 160 samples correspond to a combined length of the FFT window (128) and the cyclic prefix (32). These 160 samples are fed to a manually adjusted symbol alignment (SA) block which takes care of any arbitrary symbol timing offset induced during transmission. The SA block is manually programmed with the required timing offset value by dynamically programming the FPGA memory which sets the STO value, to obtain the minimum BER. However, this procedure can also be implemented automatically as described in [11]. The 32 cyclic prefix samples are removed to obtain the required 128 samples for input to the FFT. The FFT converts the 128 time-domain samples to 128 frequency bins. However, these 128 FFT outputs consist of both positive and negative frequencies, which are conjugate symmetric as the time-domain signal is real valued. Thus, only the 64 upper positive frequencies are extracted and fed to the functional blocks shown in Fig. 3. To simplify the implementation for the experiment, the functional block of Fig. 3 is designed to extract only one SW. However, in practice the receiver needs to extract and process all the SWs received from the transmitter. As shown in Fig. 3 the incoming 64 positive frequency subcarriers consist of 32 lower frequency subcarriers (baseband) and 32 higher frequency subcarriers (passband). The SW selection block chooses either the lower or higher frequency 32 subcarriers depending upon the SW select input. The value of the select input thus determines which of the SWs of the received OFDM signal is processed. Due to the up-sampling induced double sideband (DSB) spectral images generated at the transmitter, each SW consists of lower frequency subcarriers (SC:1 – SC:15) and high frequency subcarriers (SC:15 – SC:1) located in the lower sideband (LSB) and upper sideband (USB) respectively, ignoring any transmission-induced distortions or noise, the sidebands carry the same information as they are conjugate symmetric i.e., LSB = USB*. The corresponding LSB and USB subcarriers are equalized and undergo joint sideband processing (JSP). The method for equalization is based on the transmission of pilot subcarriers with known amplitude and phase to estimate the channel transfer function (CTF). The inverse of the estimated CTF is multiplied with the frequency domain complex data to extract the equalized k^{th} subcarrier. The MUX shown in Fig. 3 enables the dynamic selection of any of the sidebands (LSB, USB and JSP) for subsequent demapping and BER processing. Without including JSP, either the LSB or USB can be selected, therefore, at the OLT the SNR for the selected subcarrier is given by

$$SNR_{k,m,w} = \frac{\sigma^2_{X_{k,m,w}}}{\sigma^2_{N_{k,m,w}}} = \frac{E\left\{|X_{k,m,w}|^2\right\}}{E\left\{|N_{k,m,w}|^2\right\}} \quad (1)$$

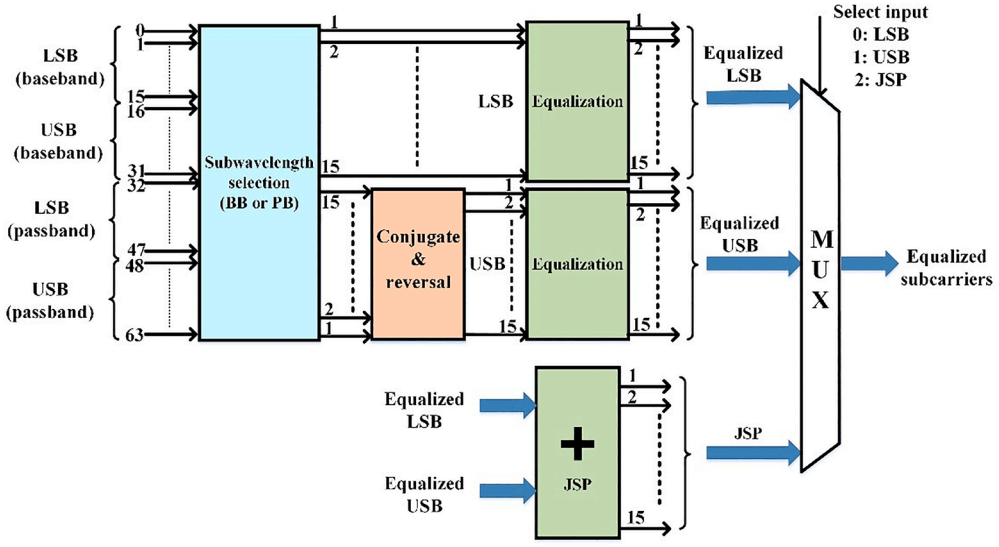

Fig. 3. Subwavelength/sideband selection and joint sideband processing.

Where $\sigma^2_{X_{k,m,w}}$, and $\sigma^2_{N_{k,m,w}}$ are the signal and noise power respectively at the specific subcarrier, k is the subcarrier index, m is the SW index (baseband or passband in the present case) and w is the sideband selected for further processing. As the selected signal is a complex valued frequency component, $|X_{k,m,w}|$ and $|N_{k,m,w}|$ denote the amplitude of signal and noise respectively. During JSP, the individual sidebands are summed coherently by adding the corresponding subcarriers from LSB and USB. However, this addition is performed after conjugating the USB. Therefore, the resultant complex frequency domain signal after performing JSP can be expressed as

$$\boldsymbol{JSP}_{k,m} = (\boldsymbol{X}_{k,m,L} + \boldsymbol{N}_{k,m,L}) + (\boldsymbol{X}_{k,m,U} + \boldsymbol{N}_{k,m,U})^* \quad (2)$$

By taking into consideration the conjugate symmetry of the LSB and USB and assuming additive white Gaussian noise, the noise at the different subcarriers becomes uncorrelated. Therefore, the signal power after JSP is given by

$$\boldsymbol{\sigma}^2_{X_{JSP_{k,m}}} = \boldsymbol{E}\left\{ \left| X_{JSP_{k,m}} \right|^2 \right\} = \boldsymbol{E}\left\{ \left| X_{k,m,L} + X^*_{k,m,U} \right|^2 \right\} = 4\boldsymbol{\sigma}^2_{X_{k,m,w}} \quad (3)$$

whereas, assuming equal noise power in the sidebands, the total noise power after JSP is

$$\boldsymbol{\sigma}^2_{N_{JSP_{k,m}}} = \boldsymbol{E}\left\{ \left| N_{JSP_{k,m}} \right|^2 \right\} = \boldsymbol{E}\left\{ \left| N_{k,m,L} + N^*_{k,m,U} \right|^2 \right\} = 2\boldsymbol{\sigma}^2_{N_{k,m,w}} \quad (4)$$

From Eq. (3) and Eq. (4) it is clear that after performing JSP the signal power increases by a factor of 4 whereas the noise power increases only by a factor of 2. Theoretically, this implies that the total SNR increases by a factor of 2 which is equivalent to a 3 dB improvement in the electrical domain and 1.5 dB improvement in the optical domain. However, the actual improvement can be less due to factors such as the channel roll-off and channel noise spectral characteristics, which can mean different SNRs for both LSB and USB. The actual improvement obtained from JSP is discussed in section 3. Further technical details regarding the JSP technique can be found in [12].

It is important to consider and compare the DSP logic resource utilization for the two implemented receiver techniques, thus the on-chip FPGA resource utilization is listed in Table 1 for both techniques when considering the total resources required for a 4 channel system. Although the resource count in Table 1 is higher for hybrid OFDM DFMA for a 4-channel system, the resource count will be highly dependent on the number of channels, and in a practical PON application the number of channels can be several 100. The resource utilization increases linearly for the DFMA receiver whereas for the hybrid OFDM DFMA receiver the complexity increases approximately logarithmically, this leads to the hybrid OFDM DFMA receiver being more computationally efficient for higher channel counts. Section 3.5 presents a detailed analysis of DSP complexity versus channel count for both techniques. The power consumption of the real-time DSP is also of interest, therefore a summary of the power consumption for both techniques is shown in Fig. 4 in terms of static, dynamic and I/O power. The two implemented techniques have a similar power consumption pattern, however as the number of channels increases the maximum clock requirement for the hybrid OFDM DFMA receiver will reduce further due to increased parallel processing in the FFT, whereas in the DFMA receiver for the same parallelization factor the clock rate required will increase. This will lead to further difference in the logic operating frequency, and combined with the lower logic resource utilization at higher channel counts, this makes the hybrid OFDM DFMA more power efficient. It should also be noted that implementation in a custom application specific integrated circuit (ASIC), will reduce power consumption significantly compared to an FPGA.

Table 1
FPGA resource utilization of a 4-channel DFMA and hybrid OFDM DFMA receiver DSPs.

Resource	DFMA	Hybrid OFDM DFMA
Adaptive logic modules (ALM)	145,144	184,554
Combinational ALUTs	158,044	264,959
Dedicated logic registers	313,760	297,495
Block memory bits	30,833,152	7,946,030
M20Ks (Dual port memory blocks)	1,948	1,260
DSP blocks	1,320	766
Logic utilization	55 %	70 %

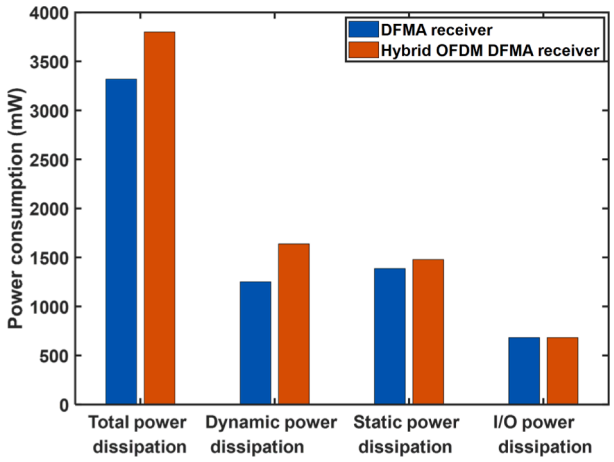

Fig. 4. FPGA power consumption for receiver DSP of DFMA and hybrid OFDM DFMA.

3. Experimental validation and results

3.1. Experimental system setup

The experimental set up for the hybrid OFDM DFMA PON is shown in Fig. 5(a). The setup is designed for the upstream transmission with all associated parameters listed in Table 2. The two physical connections from ONU 1 to the OLT and from ONU 2 to the OLT are kept identical with a nominal optical wavelength of 1550 nm for operation and a wavelength (frequency) spacing of 0.4 nm (50 GHz) to avoid the optical beating interference (OBI) effect [13]. It should be noted that in practice, the temperature controllers for the ONU lasers can be used to adjust and stabilize their wavelengths appropriately, with the OLT managing the ONU wavelength adjustments. Alternatively, techniques can potentially be used to mitigate the OBI effect [14 15], which are applicable to hybrid OFDM DFMA PONs and so can remove the requirement of ONU laser wavelength tuning. The component descriptions hereafter are the same for both the physical connections. The output electrical signal from the DAC in the transmitter (refer Fig. 2) is fed to a MX35D linear transmitter to generate an intensity modulated optical signal. The MX35D linear transmitters are an integrated system with both a tunable laser source and a lithium niobate (LiNbO3) Mach-Zehnder intensity modulator (MZM) with a bias controller. The RF signal is the only required input signal to the MX35D and the MZM is operated at the quadrature point. An EDFA is used to boost the optical output power, followed by an optical band pass filter (OBPF) to filter out the out-of-band amplified spontaneous emission (ASE) noise.

The spectra of the optical signals from ONU 1 (baseband signal) and ONU 2 (passband signal) are shown in Fig. 5(b) and (c) respectively with the insets clearly showing the baseband and passband signals respectively. The optical signals from the individual ONUs are combined using a 3 dB optical coupler (see Fig. 5(d)) and transmitted through a 26 km SSMF fiber. The combined optical signal is converted back to an AC coupled electrical signal proportional to the optical intensity by a PIN with an integrated *trans*-impedance amplifier (TIA). The analogue signal amplitude is optimized using the subsequent RF gain and attenuator stages and a low pass filter (LPF) with a bandwidth of 1 GHz to filter out

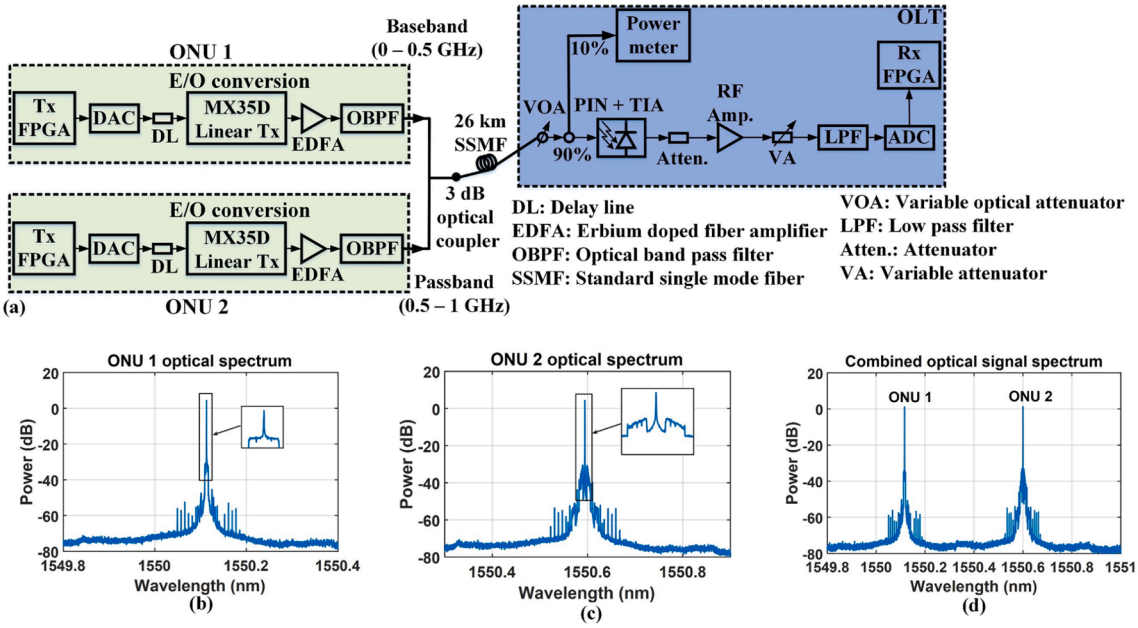

Fig. 5. (a) Experimental set up for the hybrid OFDM DFMA PON system, (b) optical spectrum for ONU 1 (baseband signal, after OBPF), (c) optical signal for ONU 2 (passband signal, after OBPF) and (d) optical spectrum for the combined optical signal (after 3 dB optical coupler).

Table 2
System parameters for Hybrid OFDM DFMA PON.

Parameter	Value
IFFT/FFT size	32/128
Number of subcarriers per channel (SC:1 – SC:15)	15
Subcarrier spacing	15.625 MHz
Total samples per symbol	40 (32 samples/symbol + 8 cyclic prefix)
Modulation format	16-QAM to 64-QAM
DAC/ADC sample rate	2 GS/s (8 - bit)
Adopted FEC limit	1×10–3
Net bit rate per channel (16-QAM, 14 subcarriers enabled)	0.7 Gb/s
Launch power after OBPF	4.5 dBm
Channe1 & 2 optical wavelength	1550.1 & 1550.5 nm
OBPF parameters	Tunable range = 1510 to 1590 nm, FWHM* @ 1550 nm = 1.02 nm
SSMF length	26 km
PIN bandwidth	40 GHz
PIN responsivity	0.7 A/W
Base clock rate	12.5 MHz
Amplitude at ADC input	$\approx 400\ mV_{pp}$

*FWHM – Full width at half maximum.

the out-of-band noise. The filtered analogue RF signal is digitized through an ADC and fed to the receiver FPGA. The performance of the system is first analyzed with a PTP configuration and directly compared with the DFMA receiver based on MFs, under the exact same conditions, to observe the DSP-induced performance enhancement. The PTP configuration adopted here is as described in section 3.1, however only ONU 1 and the OLT are connected whilst removing the 3 dB optical coupler. Hereafter, PTP will imply the aforementioned link and more importantly, the real-time hybrid OFDM DFMA PON is also validated for the MPTP configuration and again compared with the corresponding DFMA PON. It should be highlighted, that although two ONUs are employed here, a suitably large number of ONUs can be used in practice.

3.2. Performance in point-to-point links

3.2.1. PTP performance analysis

The BER performance against received optical power (ROP) is examined by adjusting the ROP at the OLT receiver via a VOA. The FEC limit adopted throughout the paper to determine minimum required ROP is 1×10^{-3}. The BER performance curves for cosine baseband, cosine passband, sine baseband and sine passband are shown in Fig. 6 (a), (b), (c) and (d) respectively. To obtain the results of Fig. 6, the PTP link is optimized for the minimum BER values for all the subcarriers by removing any STOs, using the aforementioned manual symbol timing adjustment. The performance is then evaluated for the 14 highest frequency subcarriers (SC:2 – SC:15) whilst ignoring the 1st subcarrier as it lies on the edge of the filter response and does not perform well as compared to the other subcarriers due to the non-ideal implementation of the filters. The same number of subcarriers is adopted hereafter for further investigations. The BER values in Fig. 6 are total channel BERs, obtained after averaging the individual subcarriers BERs. The study for the different channels looks at the following cases: 1) Difference in the performance of LSB and USB (adjacent SW is off), 2) Improvement obtained due to JSP and 3) Effect of interference from the other SW's channel for the JSP case. To study the interference, the RF signal input from the interfering channel is only switched on/off through the DSP function. The DSP in the ONU transmitter can generate two channels wherein one must be an I channel and the other a Q channel, the channels however can be located in either baseband or passband. Therefore, the interfering channel for $I(Q)$ baseband (passband) is $Q(I)$ passband (baseband) and for $I(Q)$ passband (baseband) is $Q(I)$ baseband (passband). The results in Fig. 6 show that the USB performs better for baseband channel whereas the LSB performs better for the passband channel. Moreover, the JSP provides a maximum improvement of ~ 1 dB in the optical power budget (cosine passband, red curve) which translates to a 2 dB electrical power improvement. Furthermore, the two BER curves for the JSP case plotted with and without the adjacent SW's channel on, shows there is not any considerable inter-SW interference as there is minimal impact on the BER performance. The physical effects underpinning these observed results are discussed in detail in section 3.3.

3.2.2. Comparison with DFMA-based PTP link

In order to further prove the efficacy of the technique targeted in the paper, a comparison is performed with a PTP link employing DFMA-based channel multiplexing/demultiplexing, under identical physical

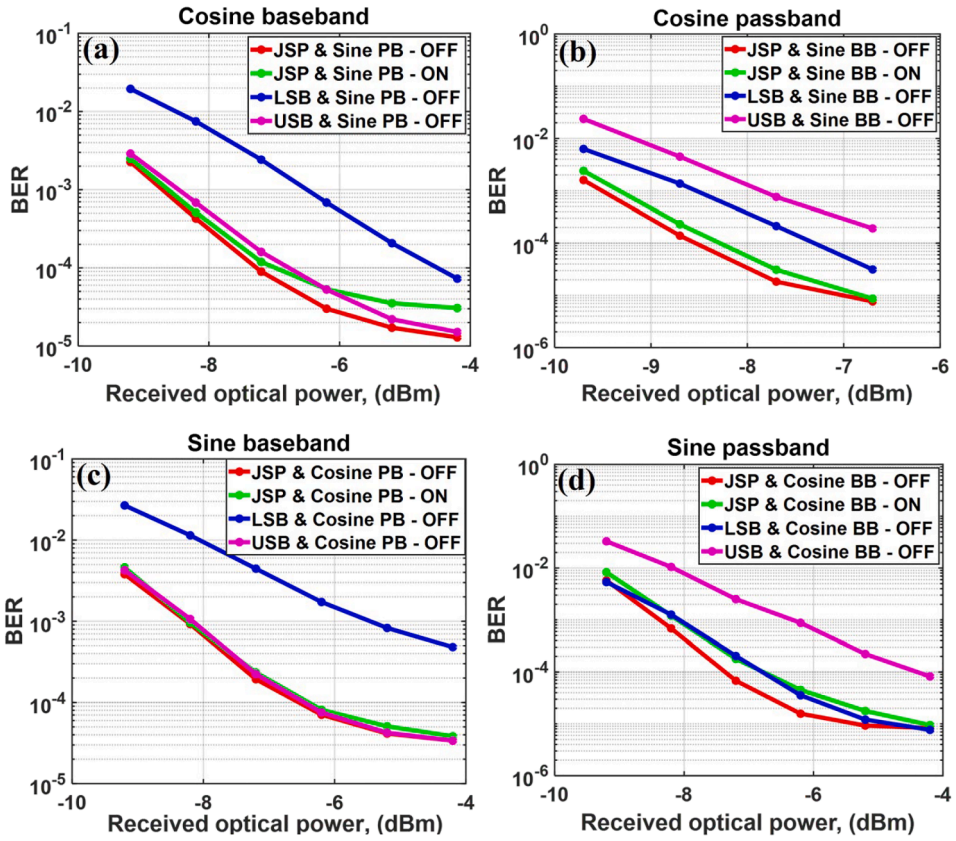

Fig. 6. BER vs ROP for the hybrid OFDM DFMA technique for PTP configuration.

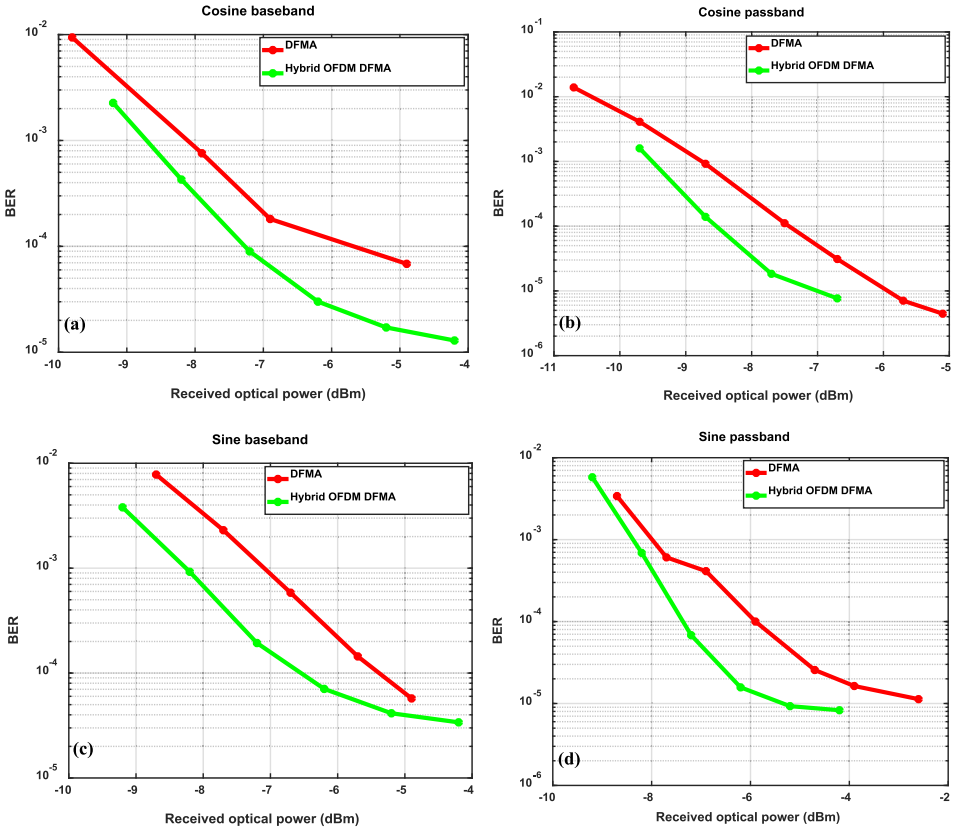

Fig. 7. Performance comparison of hybrid OFDM DFMA and DFMA.

channel conditions and DSP parameters where appropriate. To achieve a fair comparison, the receiver FPGA is simply reprogrammed with the appropriate receiver DSP without making any changes to the optical link set up. The BER is again averaged for the 14 highest frequency sub-carriers which all use 16-QAM modulation. Moreover, the power loading profile for the subcarriers is kept flat at the same power setting for both the methods and the JSP case is employed for the hybrid OFDM DFMA technique since it has been shown to offer the best performance, as discussed above. The BER curves for the four channels, for both techniques are shown in Fig. 7. Compared to the DFMA case, the hybrid OFDM DFMA case shows the best performance for all channels, the improvement in the optical power budget at the adopted FEC limit of 1×10^{-3} ranges between ≈ 0.5 dB and ≈ 1.2 dB for the sine passband and sine baseband channels respectively. The results confirm that the hybrid OFDM DFMA technique in conjunction with JSP provides enhanced performance over the DFMA technique. This agrees with the results in [9] and so confirms the ability of the hybrid OFDM DFMA PON to achieve better performance in comparison to the DFMA PON.

3.2.3. *Higher modulation format performance*

To increase the maximum achievable signal bit rate for upstream transmission the modulation format on all data carrying subcarriers (SC:2-SC:15) is changed from 16-QAM to 32-QAM. The BER performance of the PTP link for the 32-QAM modulation case is shown in Fig. 8 (a), (b), (c) and (d) for cosine baseband, cosine passband, and sine baseband and sine passband respectively. The system is thus able to offer increased signal bit rates whilst maintaining BER values below the FEC limit for a wide range of ROP. The ROP to achieve the FEC limit for all the channels is found to be −5.2 dBm, −6.2 dBm, −5dBm and −6.2 dBm respectively. In order to calculate the net signal bit rate per channel, the following equation is used [9].

$$R_b = \frac{f_{DAC}\sum_{k=1}^{N_s} n_{kb}}{2(N_s+1)(1+C_p)M} \tag{5}$$

where R_b is the net signal bit rate, f_{DAC} is the DAC sampling rate, n_{kb} is the number of bits per k^{th} subcarrier, furthermore $n_{kb} = 0$ if the k^{th} subcarrier is not used, N_s=(N/2)-1 is the total number of subcarriers with N as the IFFT size at the transmitter, C_p is the overhead factor associated with the cyclic prefix before up-sampling and M is the up-sampling factor. To obtain the new signal bit rate, a factor depending upon the cyclic prefix length is included in Eq.(5). Here the CP is chosen to be 25 %, therefore the factor is 1.25. As per Eq. (5) the raw (net) signal bit rate per channel is improved from 0.875 Gb/s (0.7 Gb/s) for 16-QAM to 1.09 Gb/s (0.875 Gb/s) for 32-QAM modulation. It can be concluded that for a PON system with 2 ONUs and a total signal bandwidth of 1 GHz, the achievable total raw (net) signal bit rate can be 2.18 Gb/s (1.75 Gb/s) when all data carrying subcarriers use 32-QAM. Although the system can perform well for 32-QAM, there is of course an associated optical power increase at the FEC limit, when compared to 16-QAM. To quantify the change in the performance for all the channels, Table 3 lists the ROPs at the adopted FEC limit for 16-QAM and 32-QAM. An average change of approximately 3 dB optical power penalty is observed, which is in accordance with the theoretical power penalty presented in [16]. The results in Fig. 8 and Table 3 also show similar behavior as the 16-QAM case with the cosine passband showing the best performance and the inter-SW effects having minimal impact on the BER performance.

The maximum demonstrated aggregate PON raw bit rate is 2.18 Gb/s, which is limited by the ADC/DAC sample rate of only 2GS/s. However, considering recent trends in integrated ADC/DAC cores, sampling speeds of the order of 64 GS/s are now commercially available [17], the available bandwidth can thus be increased by a factor of 32, thereby increasing the maximum aggregated raw bit rate to ~ 70 Gb/s when all SCs are modulated with 32-QAM. Taking into consideration channel impairments such as the channel fading effect associated with IM-DD systems, the total aggregated bit rate of the PON will be below 70 Gb/s, however, assuming an average assignment of 4-bits per SC, the

Table 3
ROP Penalty at FEC limit (1×10^{-3}) for 16-QAM and 32-QAM.

Channel	ROP (16-QAM)	ROP (32-QAM)
Cosine baseband	−8.8 dBm	−5.2 dBm
Cosine passband	−9.5 dBm	−6.2 dBm
Sine baseband	−8.3 dBm	−5 dBm
Sine passband	−8.5 dBm	−6.2 dBm

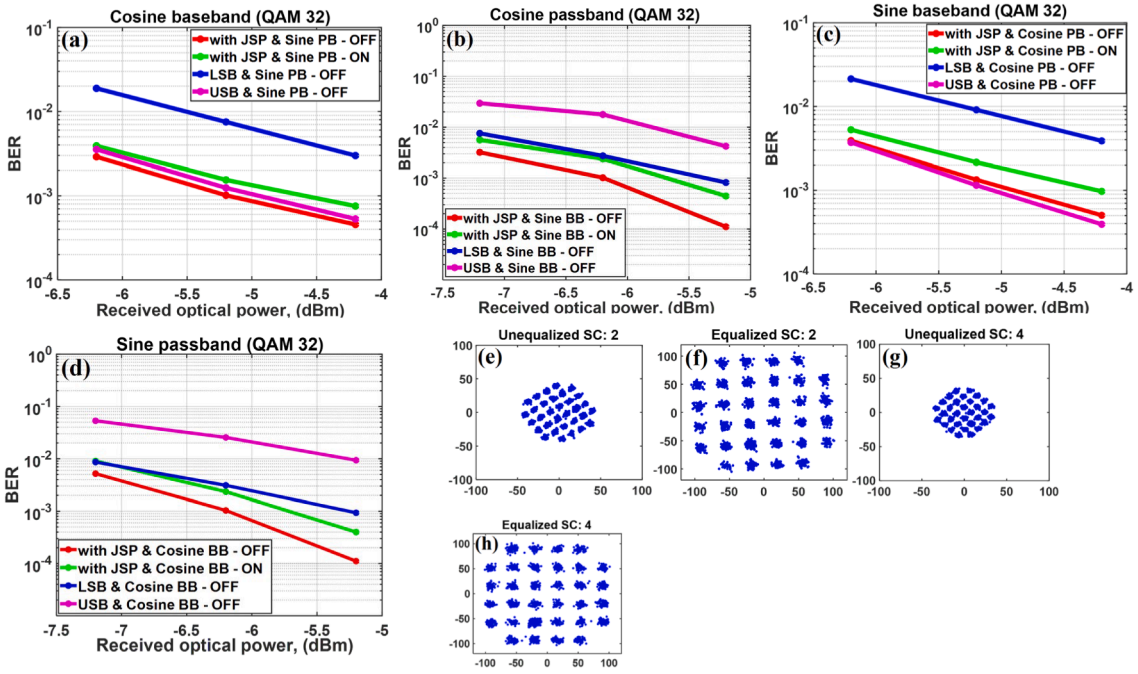

Fig. 8. The performance for 32-QAM modulation on all subcarriers for (a) cosine baseband (b) cosine passband (c) sine baseband (d) sine passband. Constellation for (e) unequalised SC: 1 (f) equalized SC: 1 (g) unequalized SC: 3 (h) equalised SC: 3.

aggregated bit rate would still be in excess of 50 Gb/s. Furthermore, techniques can potentially be employed to increase the bit rate without requiring very high sample rate converters, for example, the technique in [18] generates image spectra in the 2nd Nyquist zone and uses undersampling to reduce the required ADC sampling rates, increase the power budget, and reduce system cost and power consumption. Additionally, the method to extend the sample rate of DACs as described in [19] can be used to achieve higher sample rates whilst minimizing the cost.

3.3. Hybrid OFDM DFMA PON performance analysis

The setup presented in Fig. 5(a), is used to experimentally validate the hybrid OFDM DFMA PON consisting of 2 ONUs, where one channel (*I* or *Q*) is generated per SW. This allows the following possible SW (interfering SW) combinations: cosine baseband (cosine passband), cosine passband (cosine baseband), sine baseband (sine passband) and sine passband (sine baseband). The performance of the different channels is observed for individual sidebands only (LSB or USB) and for JSP with and without interference from the neighboring SW, the results are shown in Fig. 9. As in the case of the PTP link, to study the interference the signal is switched on/off from the DSP only, thus the unmodulated optical carrier is still present. Therefore, it is important to note that the ROP values in Fig. 9 are the total ROP values at the OLT i.e., the combined power from both ONU1 and ONU2, so the individual ROP for each ONU is 3 dB less than the total ROP as each ONU transmits the same optical launch power. Furthermore, for the LSB and USB performance evaluation, the interfering channel is switched off. The general trend in the results is found to be similar to the PTP case with the interfering channel not having a significant effect on the performance of the channel under test. Additionally, the sideband performance is also similar with USB and LSB performing better in the baseband and passband respectively. Moreover, the JSP can provide a maximum improvement of 1.2 dB in optical power budget for the cosine passband channel which translates to 2.4 dB in the electrical domain. This is in agreement with the results obtained in the PTP case.

To understand this difference in the performance of LSB and USB, the signal spectrum at the ADC input is analyzed. Fig. 10 shows the overlapped spectrum of both the noise floor and signal with both the SWs switched on. It is evident that the noise power increases towards the lower frequency region as compared to the higher frequency region and the signal power also rolls-off with increasing frequency. The power roll-off observed in the signal and the noise can be due to the combination of the physical channel's gain roll-off effect and the signal-to-signal beating effect occurring in the receiver. In Fig. 10, the estimated SNRs for LSB (11 dB and 16 dB) and USB (14 dB and 13 dB) in the baseband and passband respectively are shown. These estimated SNRs agree with the observed differences in performance of each channel, i.e., the two inner sidebands with higher SNR have the better performance.

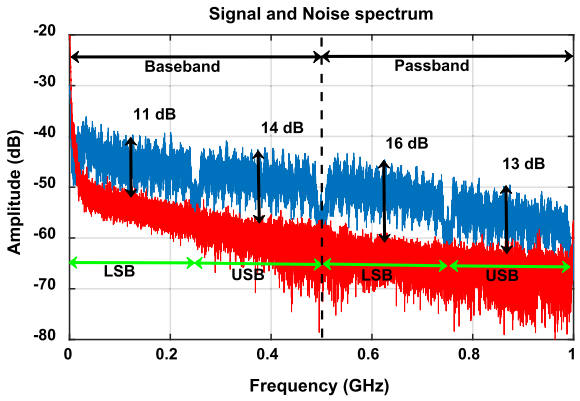

Fig. 10. Signal spectrum at the ADC input when both SWs are active.

To further investigate the effect of channel roll-off on the USB in passband, the normalized frequency response is acquired using the DSP channel estimation function. The frequency response is normalized such that the first subcarrier is located at 0 dB. The frequency response covers the whole 1 GHz range including both the channels (*I* and *Q*) and SWs (BB and PB). These frequency responses for both the SWs and channels *I* and *Q* are shown in Fig. 11. As can be observed, the higher frequency subcarriers undergo higher attenuation and the overall gain roll-off in one SW is ~ 5 dB. This result agrees with the electrical signal spectrum obtained in Fig. 10 at the ADC input.

To analyze the subcarrier dependent behavior of the hybrid OFDM DFMA PON, the BER vs subcarrier index is plotted in Fig. 12(a) – (d) for each of the four channels. The results shown are for the JSP case since it

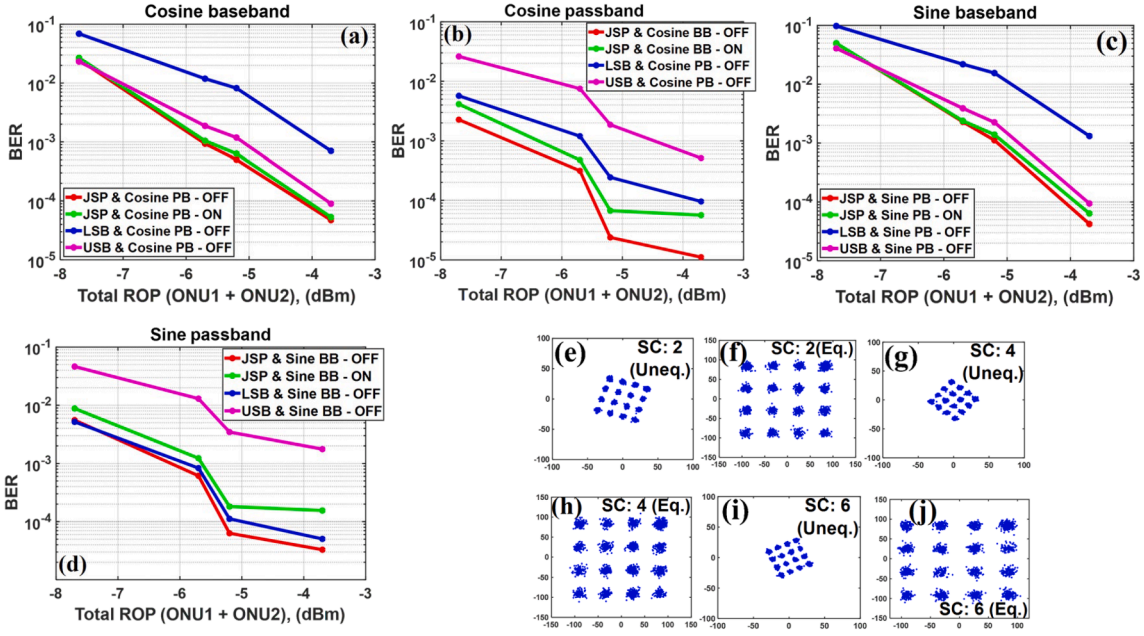

Fig. 9. ROP vs BER performance of hybrid OFDM DFMA PON system for (a) cosine baseband (b) cosine passband (c) sine baseband and (d) sine passband. Constellation diagrams for (e) unequalized SC:2 (f) equalized SC:2 (g) unequalized SC:4 (h) equalized SC:4 (i) unequalized SC:6 and (j) equalized SC:6.

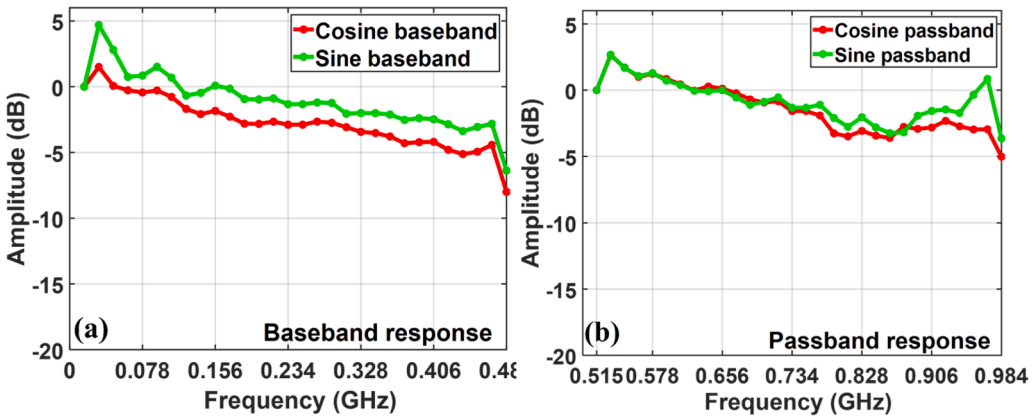

Fig. 11. Normalized frequency response for I and Q channels for both (a) baseband and (b) passband.

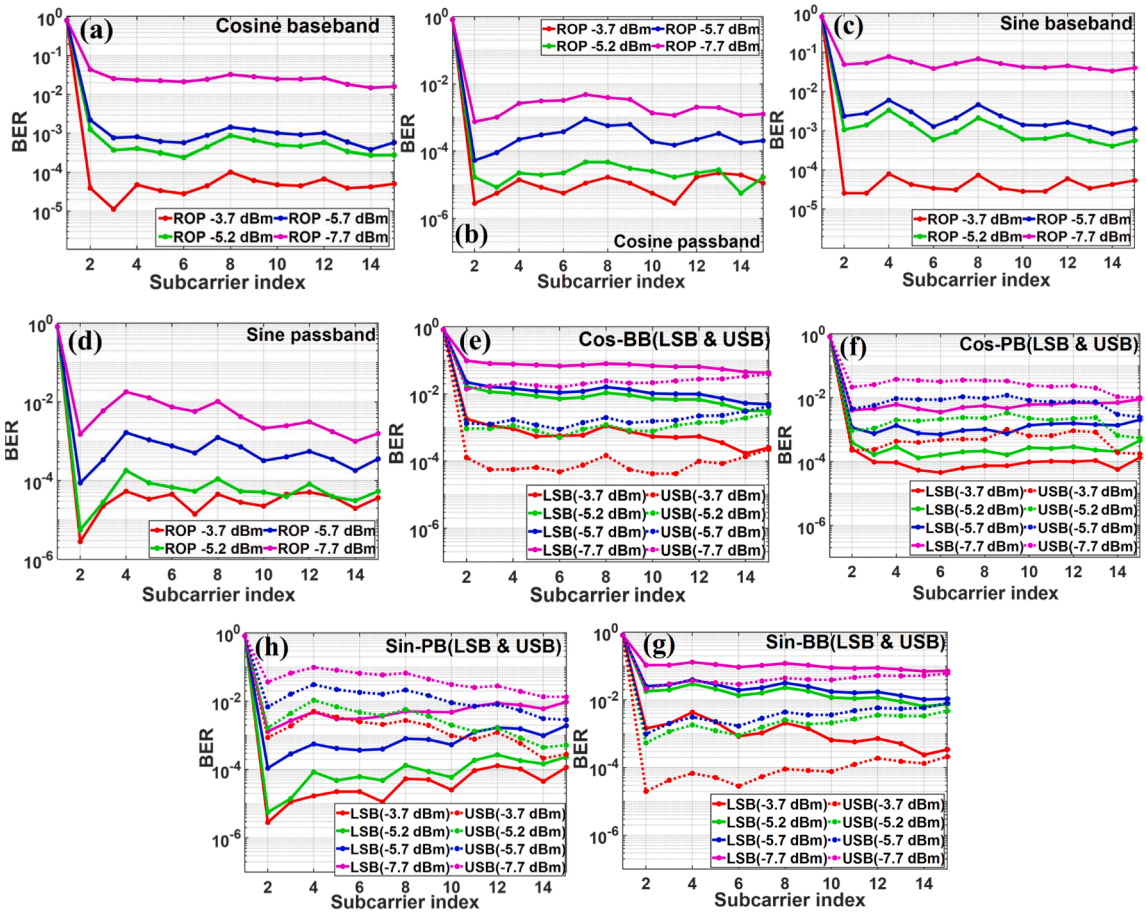

Fig. 12. BER vs subcarrier index for (a) cosine baseband (JSP) (b) cosine passband (JSP) (c) sine baseband (JSP) (d) sine passband (JSP) (e) Cos-BB (LSB & USB) (f) Cos-PB (LSB & USB) (g) Sin-BB (LSB & USB) and (h) Sin-PB (LSB & USB).

is able to provide better performance in some cases. The operating conditions are the same as PTP i.e. SC:1 power = 0 and the interfering SW band is off. The plots show subcarrier performance for different ROP values of −3.7 dBm, −5.2 dBm, −5.7 dBm and −7.7 dBm. Fig. 12(a) – (d) show that as the ROP reduces the BER performance degrades, as expected, however, the BER curves are reasonably flat and do not show significant subcarrier dependent behavior, despite the roll-off observed in the received electrical signal's power spectrum. Furthermore, the subcarrier dependent performance is also shown for the individual sidebands (LSB & USB) for each of the channels in Fig. 12(e) – (h) (LSB - solid lines, USB- dashed lines). It can be seen that for the case of detecting a single sideband there can be a large difference between the LSB and USB performance, for example for the sine passband channel in Fig. 12(h), at −3.7dBm ROP, the LSB (USB) has an increasing (decreasing) BER trend with subcarrier index, with the BER of some subcarriers in the USB exceeding the adopted FEC limit. However, for this channel, when JSP is employed, as shown in Fig. 12(d), the variation in BER with subcarrier index is reduced and so the JSP technique has the advantage of equalizing the BER performance across all subcarriers. This effect is because the recovered subcarriers with JSP are a combination of the LSB and USB subcarrier pairs, and the LSB and USB subcarriers have opposite BER vs subcarrier index trends, thus upon coherent addition

with JSP the trends in the sidebands tend to cancel out leading to an almost frequency independent behavior.

3.4. Tolerance to STO

The robustness of the real-time hybrid OFDM DFMA PON to STO at the OLT receiver is analyzed by observing the BER against the STO value. To do this, the PTP configuration, as described in section 3.1, is employed. ONU1 and the OLT are first synchronized to give a minimum BER performance, thus an optimum STO. Thereafter, a specific STO is manually forced through the DSP symbol alignment function in the ONU, which can adjust the digital signal delay in multiples of one sample interval. The STO is adjusted over a range of 0 to 39 samples, thus exceeding the length of the CP (32 samples). The 14 highest frequency subcarriers are enabled and the average BER is monitored, the STO range which maintains the BER below the FEC limit, thus indicates its robustness to the STO. This procedure is performed for both the PTP DFMA and PTP hybrid OFDM DFMA setups to allow comparisons of the STO tolerance. The comparative results in Fig. 13 show that the hybrid OFDM DFMA PON is significantly more robust to STO variation and can tolerate an STO range of approximately 30 samples, which is close to the effective length of the cyclic prefix after up-sampling ($8 \times 4 = 32$). This range can be explained by the fact that the CP provides a margin for the allowed symbol misalignment, the misalignment resulting in subcarrier phase shifts, which are accommodated by the channel equalization function. The range is slightly below the CP length showing there is a small level of inter symbol interference (ISI). For an STO beyond 32 samples, the captured received symbol now contains samples from two different transmit symbols, so the BER rapidly increases to very high values above the FEC limit. However, for the case of the DFMA PTP system the robustness to STO is very poor compared to the hybrid OFDM DFMA case, as peaks are observed in the BER curve (encircled in black) and the BER oscillates between low values below the FEC limit and excessively high values. The successive BER peaks are spaced every 4 samples, which is also the employed up-sampling factor. The BER oscillation occurs because the changing STO is causing the incoming signal and the MF to go in and out of orthogonality, when maximum orthogonality is achieved, an STO change of M ($M/2$) causes the orthogonality to be restored (fully destroyed). It should be noted that the BER oscillation should occur over a region of similar length to the CP, the curves in Fig. 13 do not show this due to the arbitrary nature of the STO at system power up. For the case of the PTP hybrid OFDM DFMA link, due to the absence of MF no such BER peaks are present as the STO cannot cause loss of orthogonality and simply results in subcarrier phases changes which are mitigated by the channel equalization. This analysis clearly demonstrates the superior tolerance of the hybrid OFDM DFMA systems to STO compared to the DFMA-based systems.

3.5. DSP complexity analysis

In this section, the DSP complexity of the OLT receiver is analyzed and compared for the cases of the hybrid OFDM DFMA PON and the DFMA PON. In the DFMA receiver the MF must achieve the same sample throughput as the ADC sample rate, whereas the FFTs are after the $M\times$ down-sampling so operate at a sample throughput $M\times$ lower. To perform a fair comparison, the number of scalar multipliers to process one symbol is considered as a measure of complexity as these are the most abundant functional elements in the FFTs and the filters and consume significantly more logic resources than the adders. For this purpose, the two systems under comparison consist of the same number of channels B and the same number of subcarriers per channel thus IFFT size at the ONU transmitter is N. For the DFMA PON OLT receiver each channel needs a MF and a corresponding FFT operation. Therefore, for example a 4-channel DFMA PON will require 4 MFs and 4 FFTs. To

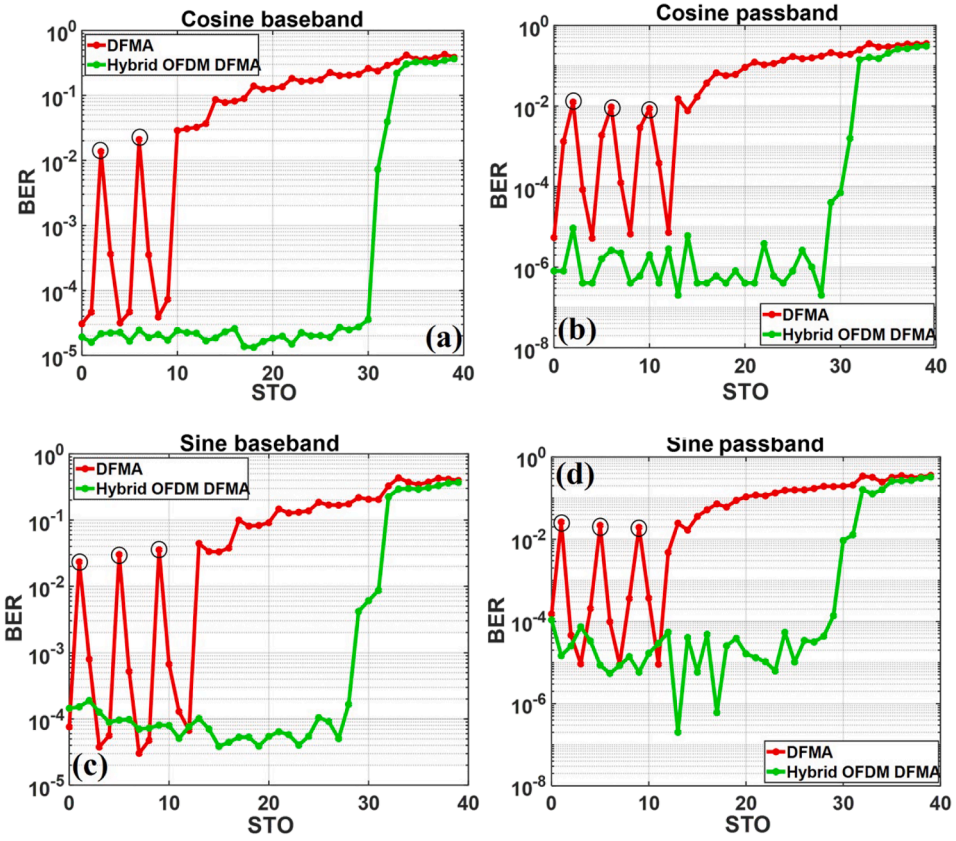

Fig. 13. Comparative study for tolerance to symbol timing offset for DFMA and Hybrid OFDM DFMA for (a) cosine baseband (b) cosine passband (c) sine baseband and (d) sine passband.

generalize, the total number of complex multipliers in all the FFTs for DFMA PON case is given by:

$$CM_{dfma} = B \times \left(\frac{N}{2}\right) \times log_2 N \tag{6}$$

Since each complex multiplication is equivalent to 4 scalar multiplications, the complex multiplications can be easily converted to an equivalent number of scalar multiplications. The complexity for the MF is also determined by the number of scalar multipliers required. It should be noted that the effective length for the matching filter is also dependent upon the up-sampling factor M. An in-depth analysis with MF design guidelines is described in [20] and recommends an optimum MF tap length $T = 16 \times M$. Considering the tap length of the MF, the total number of multiplications required to process one channel within one symbol is $16 \times M$, where $M = 2B$. Therefore, considering all channels, the generalized expression for complexity of the MFs in terms scalar multipliers (SM) becomes.

$$SM_{MF} = B \times T = B \times 16(2B) = 32B^2 \tag{7}$$

Therefore, the total complexity for the DFMA receiver inclusive of the FFTs and MFs in terms of equivalent scalar multiplications is given by:

$$SM_{dfma} = \left[4 \times B \times \left(\frac{N}{2}\right) \times log_2 N\right] + \left(32B^2\right) \tag{8}$$

The first term in Eq. (8) represents the FFT complexity and the multiplier of 4 is to get the equivalent scalar multipliers. On the other hand, the hybrid OFDM DFMA PON eliminates the MFs removing the 2nd term in Eq. (8) while the 1st term is retained as a single FFT operation given by:

$$CM_{hybrid} = \left(\frac{L}{2}\right) \times log_2 L \tag{9}$$

where $L = MN = 2BN$. Note, these are again complex multiplications and to get an equivalent scalar multiplier count a multiplication with 4 is required which changes Eq. (9) to.

$$SM_{hybrid} = 4 \times BNlog_2 2BN \tag{10}$$

The Eq. (8) and Eq. (10) are computed for different values of channel count B with fixed IFFT size $N = 32$ at the transmitter and filter length of 16 and plotted in Fig. 14. The result shows that as the number of channels increase the complexity of the OLT receiver in a DFMA PON scales up at a significantly faster rate than for the hybrid OFDM DFMA PON. The difference in complexity increases further as the number of channels increase with the hybrid OFDM DFMA receiver offering ≈ 5 times less complexity as compared to DFMA for a channel count of 256.

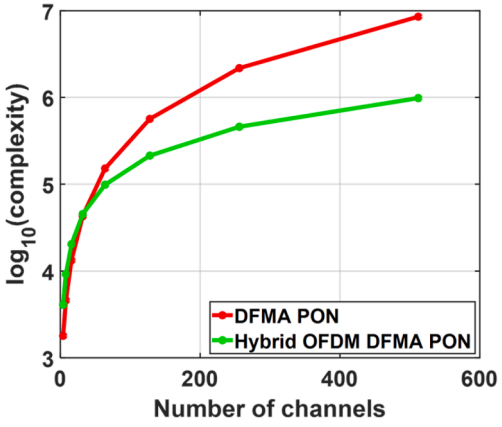

Fig. 14. Complexity (number of scalar multipliers) variation with channel count.

A brief comparison between the two PON OLT receiver techniques is presented in Table 4. It is also worth highlighting that the maximum clock rate requirement for the demonstrated hybrid OFDM DFMA case is drastically reduced from 125 MHz to 12.5 MHz (at a 2GS/s sample rate) in comparison to the DFMA PON case. This requirement reduces further for the hybrid OFDM DFMA receiver as the number of channels increases since it leads to increased parallel processing in the FFT. However, for the DFMA receiver, for a fixed parallelization factor (number of parallel filters) the clock speed requirement increases further. This further increases the difference between the logic clock rate requirement of the two techniques, which will obviously have a significant impact on the digital logic power requirements.

4. Conclusion

A real-time hybrid OFDM DFMA PON has been functionally validated with transmission over 26 km SSMF, while achieving dynamic network reconfigurability. A joint sideband processing technique is demonstrated to provide a maximum improvement in optical power budget of 1 dB in the PTP configuration and 1.2 dB in the PON configuration. When compared to a DFMA-based system the demonstrated technique provides a best-case improvement of 1.2 dB in optical power budget with 14 active subcarriers per channel. The difference in performance of LSB and USB in both SWs was shown to be attributed to the quite large variation in the channel SNRs. However, the JSP is able to mitigate these effects and is able to provide both an enhanced overall channel BER performance and to equalize the BER performance across subcarriers. Moreover, the hybrid OFDM DFMA is much more tolerant to the STO with the range of tolerance equal to the margin provided by the cyclic prefix, whereas the DFMA-based system suffers from the major drawback of high sensitivity to STO as a small STO (dependent upon the up-sampling factor) can lead to loss of orthogonality which results in unacceptably high BER. Finally, from the point of view of implementation in a cost and power efficient system on chip (SoC) device, the demonstrated technique not only reduces the computational complexity by factors of the order of $\times$ 5 or more, for high channel counts, but also drastically reduces the maximum clock rate requirement which significantly reduces the power requirement. The maximum achievable aggregate bit rate is limited by the ADC/DAC sampling speed, however new high speed state-of-the-art ADCs/DACs are able to mitigate this limitation. A real-time hybrid OFDM DFMA PON with two orthogonal channels in a single subwavelength band is under investigation as it can lead to increased spectral efficiency. The real-time demonstration of the hybrid OFDM DFMA PON is a key milestone in verifying its technical feasibility to provide SDN-controlled physical layer network reconfigurability to offer highly efficient use of network resources, elastic bandwidth provisioning and convergence of fixed and mobile networks.

Funding

This work was supported by the DSP Centre of Excellence funded by the European Regional Development Fund (ERDF) through the Welsh Government.

Table 4
Comparison summary between DFMA and Hybrid OFDM DFMA PON.

Parameter	DFMA PON [8]	Hybrid OFDM DFMA PON
Maximum required clock rate (for 4 channels)	125 MHz	12.5 MHz
Number of FFTs required	'B' number of N point FFTs	Single ($M \times N$) point FFT
Matching filters	One per channel	Not required
Overall complexity (in terms of scalar multipliers)	$4 \times \left[B \times \left(\frac{N}{2}\right) \times \log_2 N\right] + (32B^2)$	$4BN\log_2 BN$

CRediT authorship contribution statement

Tushar Tyagi: Conceptualization, Methodology, Investigation, Validation, Writing – original draft. **Roger Giddings:** Funding acquisition, Project administration, Conceptualization, Supervision, Writing – review & editing. **J.M. Tang:** Funding acquisition, Conceptualization, Writing – review & editing.

Declaration of Competing Interest

The authors declare the following financial interests/personal relationships which may be considered as potential competing interests: Roger Giddings reports financial support was provided by European Regional Development Fund.

Data availability

The data that has been used is confidential.

References

[1] Ciena, Introducing the Adaptive Network Vision, 2018. https://media.ciena.com/documents/Introducing-the-Adaptive-Network-Vision-WP.pdf.

[2] P.T. Dat, A. Kanno, N. Yamamoto, T. Kawanishi, Seamless convergence of fiber and wireless systems for 5G and beyond networks, J. Light. Technol. 37 (2019) 592–605, https://doi.org/10.1109/JLT.2018.2883337.

[3] R. Giddings, Real-time digital signal processing for optical OFDM-based future optical access networks, J. Light. Technol. 32 (2014) 553–570, https://doi.org/10.1109/JLT.2013.2281628.

[4] N. Cvijetic, OFDM for next-generation optical access networks, J. Light. Technol. 30 (2012) 384–398, https://doi.org/10.1109/JLT.2011.2166375.

[5] M. Bolea, R.P. Giddings, J.M. Tang, Digital orthogonal filtered optical OFDM for elastic PONs, Opt. Fiber Commun. Conf. OFC 2014 (32) (2014) 1200–1206, https://doi.org/10.1364/ofc.2014.w2a.24.

[6] X. Duan, R.P. Giddings, S. Mansoor, J.M. Tang, Experimental demonstration of upstream transmission in digital filter multiple access pons with real-time reconfigurable optical network units, J. Opt. Commun. Netw. 9 (2017) 45–52, https://doi.org/10.1364/JOCN.9.000045.

[7] C. Zhang, Y. Yan, T. Wu, X. Zhang, G. Wen, K. Qiu, Phase masking and time-frequency chaotic encryption for DFMA-PON, IEEE Photonics J. 10 (2018) 1–9, https://doi.org/10.1109/JPHOT.2018.2852299.

[8] E. Al-Rawachy, R.P. Giddings, J. Tang, Experimental Demonstration of a Real-Time Digital Filter Multiple Access PON With Low Complexity DSP-Based Interference Cancellation, J. Light. Technol. 37 (2019) 4315–4329, https://doi.org/10.1109/jlt.2019.2923546.

[9] Y. Dong, R.P. Giddings, J. Tang, Hybrid OFDM-digital filter multiple access PONs, J. Light. Technol. 36 (2018) 5640–5649, https://doi.org/10.1109/JLT.2018.2877840.

[10] W. Jin, Z.Q. Zhong, J.X. He, A. Sankoh, R.P. Giddings, Y.H. Hong, I. Pierce, M. O'Sullivan, C. Laperle, J. Lee, G. Mariani, T. Durrant, J.M. Tang, Experimental Demonstrations of Hybrid OFDM-Digital Filter Multiple Access PONs, IEEE Photonics Technol. Lett. 32 (2020) 751–754, https://doi.org/10.1109/LPT.2020.2995072.

[11] X.Q. Jin, R.P. Giddings, E. Hugues-Salas, J.M. Tang, Real-time experimental demonstration of optical OFDM symbol synchronization in directly modulated DFB laser-based 25km SMF IMDD systems, Opt. Express 18 (2010) 21100, https://doi.org/10.1364/oe.18.021100.

[12] O.F.A. Gonem, R.P. Giddings, J. Tang, Timing Jitter Analysis and Mitigation in Hybrid OFDM-DFMA PONs, IEEE Photonics J. 13 (2021) 1–13, https://doi.org/10.1109/JPHOT.2021.3121168.

[13] S.M. Jung, K.H. Mun, S.Y. Jung, S.K. Han, Optical-Beat-Induced Multi-User-Interference Reduction in Single Wavelength OFDMA PON Upstream Multiple Access Systems with Self-Homodyne Coherent Detection, J. Light. Technol. 34 (2016) 2804–2811, https://doi.org/10.1109/JLT.2016.2551295.

[14] S.-Y. Jung, C.-H. Kim, S.-M. Jung, S.-K. Han, Optical pulse division multiplexing-based OBI reduction for single wavelength uplink multiple access in IM/DD OFDMA-PON, Opt. Express 24 (2016) 29198, https://doi.org/10.1364/oe.24.029198.

[15] H.J. Park, C.H. Kim, S.Y. Jung, S.K. Han, A novel OBI noise reduction technique by using similar-OBI estimation in optical multiple access uplink, Int. Conf. Transparent Opt. Networks. 25 (2017) 20860–20865, https://doi.org/10.1109/ICTON.2017.8024890.

[16] J.M. Tang, K.A. Shore, Maximizing the transmission performance of adaptively modulated optical OFDM signals in multimode-fiber links by optimizing analog-to-digital converters, J. Light. Technol. 25 (2007) 787–798, https://doi.org/10.1109/JLT.2006.890457.

[17] Intel® FPGA with Integrated ADC/DAC Technology, (n.d.). https://www.intel.co.uk/content/www/uk/en/architecture-and-technology/programmable/analog-rf-fpga.html#:~:text=Introducing Intel® FPGA with,end test and wireless solutions.

[18] Y. Liu, Q. Chen, Real time GB OFDM signal generation/reception using image spectra and undersampling for IMDD system, (2022) 8–11. https://doi.org/10.1109/LPT.2022.3197828.

[19] C. Laperle, M. Osullivan, Advances in high-speed DACs, ADCs, and DSP for optical coherent transceivers, J. Light. Technol. 32 (2014) 629–643, https://doi.org/10.1109/JLT.2013.2284134.

[20] M. Bolea, R.P. Giddings, M. Bouich, C. Aupetit-Berthelemot, J.M. Tang, Digital filter multiple access PONs with DSP-enabled software reconfigurability, J. Opt. Commun. Netw. 7 (2015) 215–222, https://doi.org/10.1364/JOCN.7.000215.